Charge transfer and negative curvature energy in magnesium boride nanotubes

Hui Tang and Sohrab Ismail-Beigi

Department of Applied Physics, Yale University, New Haven, Connecticut 06520, USA
(Received 6 August 2015; revised manuscript received 13 June 2016; published 18 July 2016)

Using first-principles calculations based on density functional theory, we study the energetics and charge transfer effects in MgB_x nanotubes and two-dimensional (2D) sheets. The behavior of adsorbed Mg on 2D boron sheets is found to depend on the amount of electron transfer between the two subsystems. The amount is determined by both the density of adsorbed Mg as well as the atomic-scale structure of the boron subsystem. The degree of transfer can lead to repulsive or attractive Mg-Mg interactions. In both cases, model MgB_x nanotubes built from 2D MgB_x sheets can display negative curvature energy: a relatively unusual situation in nanosystems where the energy cost to curve the parent 2D sheet into a small-diameter nanotube is negative. Namely, the small-diameter nanotube is energetically preferred over the corresponding flat sheet. We also discuss how these findings may manifest themselves in experimentally synthesized MgB_x nanotubes.

Single-walled inorganic nanotubes based on carbon, BN, pure boron, etc., have been studied using both theory and experiments [1–7]. Such nanotubes can be constructed by starting with a precursor two-dimensional (2D) sheet, cutting out a long strip, and curving the strip to form a tubular structure. Many of the electronic properties of large-diameter nanotubes can be understood directly from the sheet precursors using zone-folding techniques [8]. However, the electronic properties of small-diameter nanotubes can be modified by strong curvature effects [9]. In addition to changing electronic properties [6,9,10], a more basic fact about curvature is its energy cost: energy is required to curve and bend the covalent bonds of the sheet to form the nanotube [6,10,11]. Viewed as an elastic effect, curvature energy is positive and its magnitude scales with nanotube diameter as the inverse second power [6,10,11].

Following the prediction and fabrication of pure boron nanotubes [4,12,13], magnesium-boride nanotubes have been systematically studied by theorists in part to find novel one-dimensional superconductors [14–20]. Experiments have shown a diamagnetic transition near 80 K in Mg boride samples which could indicate higher superconducting temperature than bulk MgB_2 [20]. A number of theoretical works have studied MgB_2 nanotubes based on a hexagonal MgB_2 precursor sheet [14–19]. Two works reported the existence of negative curvature energy in MgB_2 nanotubes but provided no underlying explanation [18,19]. Although the hexagonal MgB_2 sheet itself is not an optimal sheet [21], we show below that negative curvature energy is a common phenomenon in model Mg boride nanotubes.

In this work, we use first-principles electronic structure methods to study curvature and charge transfer effects in MgB_x sheets and nanotubes. We show that negative curvature energy is a common property in model Mg boride nanotubes (i.e., systems with small unit cells, no disorder, and no heterogeneity). We show that Mg-Mg interactions create the negative curvature energy, and these interactions depend on the degree of electron transfer between the Mg and boron subsystems. Hence, the physical basis of the phenomenon is general and may be applicable to experimentally synthesized MgB_x as well as other nanotubular materials.

Our calculations use first-principles density functional theory [22,23] within the plane-wave pseudopotential total energy approach [24] and employ the Quantum Espresso software [25]. We use the local density approximation (LDA) [23,26] for exchange and correlation and employ norm-conserving pseudopotentials [27]. For Mg, the pseudopotential is generated with reference state $3s^2 3p^3 3d^0$ and cutoff radii $(r_c^s, r_c^p, r_c^d) = (2.1, 2.5, 2.5)a_0$. For B, we use $2s^2 2p^1 3d^0$ as reference and cutoff radii $(r_c^s, r_c^p, r_c^d) = (1.7, 2.1, 1.7)a_0$. Both pseudopotentials use d as the local channel. A plane-wave basis with an energy cutoff of 32 Ry describes the Kohn-Sham wave functions. Two-dimensional (2D) calculations are performed with a slab geometry extended in the x-y plane and with 10 Å of vacuum separating periodic images along z. Nanotube calculations use a tetragonal unit cell with the nanotube axis aligned along z and a minimum of 10 Å vacuum separating periodic images in the x-y plane. K-point sampling with a Gaussian smearing width of 0.5 eV converges total energies to better than 1 meV/atom. Structural relaxations reduce all force components below 0.01 eV/Å. Lattice vectors are relaxed to reduce stresses below 100 MPa. Maximally localized Wannier functions are generated using established procedures and software packages [28–30].

Negative curvature energy in model MgB_x *nanotubes*. We start with well-defined and clean model MgB_x nanotubular systems in order to demonstrate the existence of negative curvature and isolate its underlying physical basis. Following standard definitions, the curvature energy is the energy cost to curve the parent 2D MgB_x sheet into a nanotube [7]: the energy of the nanotube minus the energy of the parent sheet with the same number of atoms.

We begin with nanotubes created out of the highly stable α boron sheet [5,6] with Mg adsorbed on its surface in a 1:8 ratio (forming MgB_8). For the controlled model calculations in this section, all the Mg are placed on one side of the B sheet prior to curving the sheet into a nanotube. (In another section below, we will consider more complex situations concerning Mg placement.) Hence, we end up with two types of nanotubes: either all the Mg are on the exterior surface of the nanotube or all the Mg are on the interior surface. Figure 1 shows the resulting curvature energies as a function of nanotube diameter for two choices of nanotube chirality. When the Mg
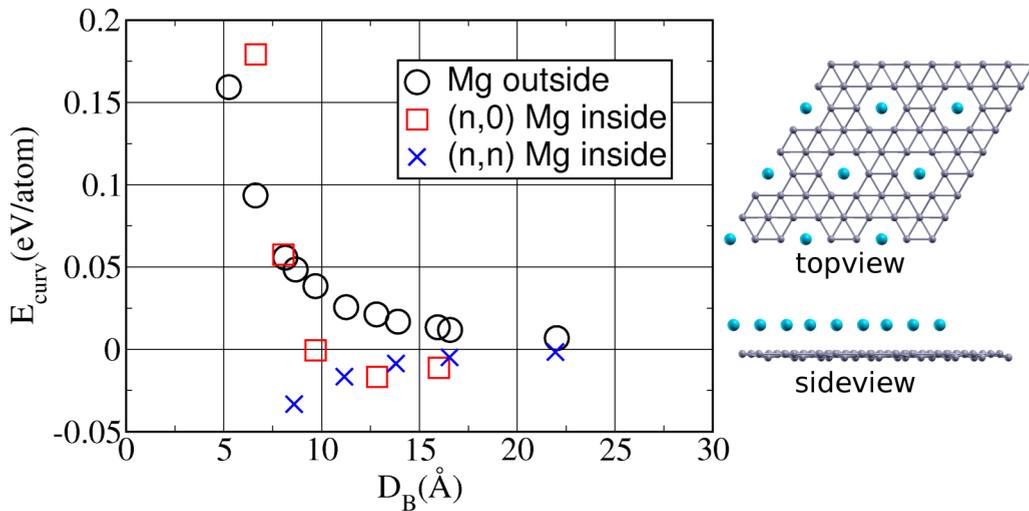
FIG. 1. Left: Curvature energy per atom versus diameter for model MgB_8 nanotubes made from the Mg-doped α sheet. The diameter refers to that of the underlying boron nanotube. Right: Structure of the MgB_8 sheet used to form these nanotubes. Large blue balls are Mg, small gray balls are B.

is outside, the curvature energies are uniformly positive and decay to zero with increasing diameter which is the standard behavior. However, nanotubes with the Mg inside display negative curvature energies for small diameters: the energy of the curved nanotube is lower than the sheet.

Next, we consider nanotubes made by curving the hexagonal boron sheet (isomorphic to graphene) again with all Mg adsorbed on the same side of the sheet at a 1:2 ratio (MgB_2 sheets and nanotubes). Figure 2 displays the resulting curvature energies: contrary to the α-sheet derived model MgB_8 nanotubes, placing the Mg inside the MgB_2 nanotubes leads to positive curvature energy while placing the Mg outside leads to negative curvature energy.

More generally, we have studied a series of Mg-doped boron sheets where the boron subsystem has hexagonal hole density η ranging from 0 (triangular) to 1/3 (hexagonal) [5]. We find that

negative curvature energy occurs for Mg-doped boron sheets over the entire range of η. In addition, we notice a simple trend: negative curvature energy occurs for small-η sheets when Mg atoms are inside the nanotubes, while for large-η sheets the Mg must be outside to deliver negative curvature energy.

To the best of our knowledge, negative curvature energy is not a common observation for nanotubular systems. Hence, it is not immediately obvious whether our finding of negative curvature energy on model nanotubes is applicable or relevant to more complex or realistic structures of MgB_x nanotubes. We first need to understand the underlying reasons and mechanisms for the negative curvature energy. This is best accomplished by focusing on the behavior of Mg atoms adsorbed on 2D boron sheets in order to understand the nature of the Mg-Mg interactions.
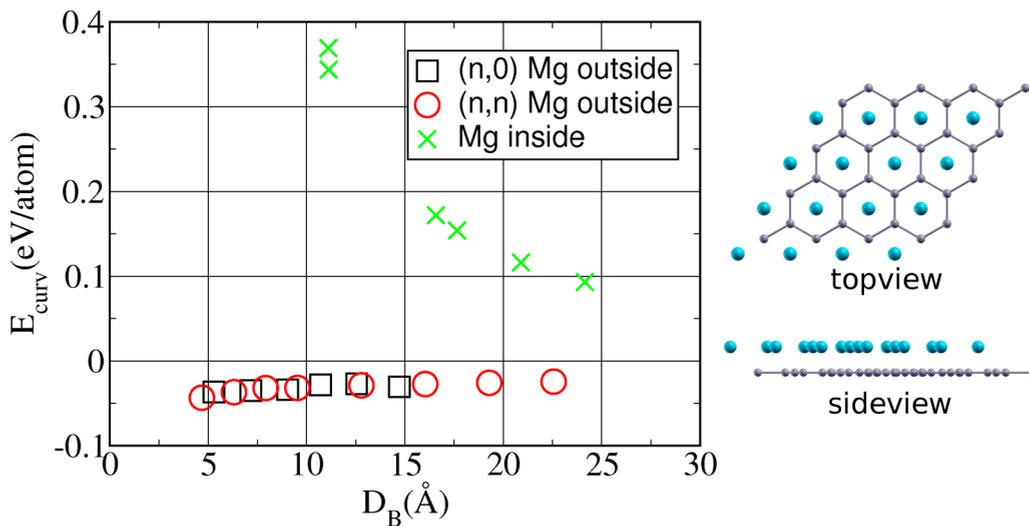
FIG. 2. Left: Curvature energy per atom versus diameter for model nanotubes made from the hexagonal MgB_2 sheet. The diameter refers to that of the underlying boron nanotube. Right: Structure of the hexagonal MgB_2 sheet used to form the nanotubes. Large blue balls are Mg, small gray balls are B.
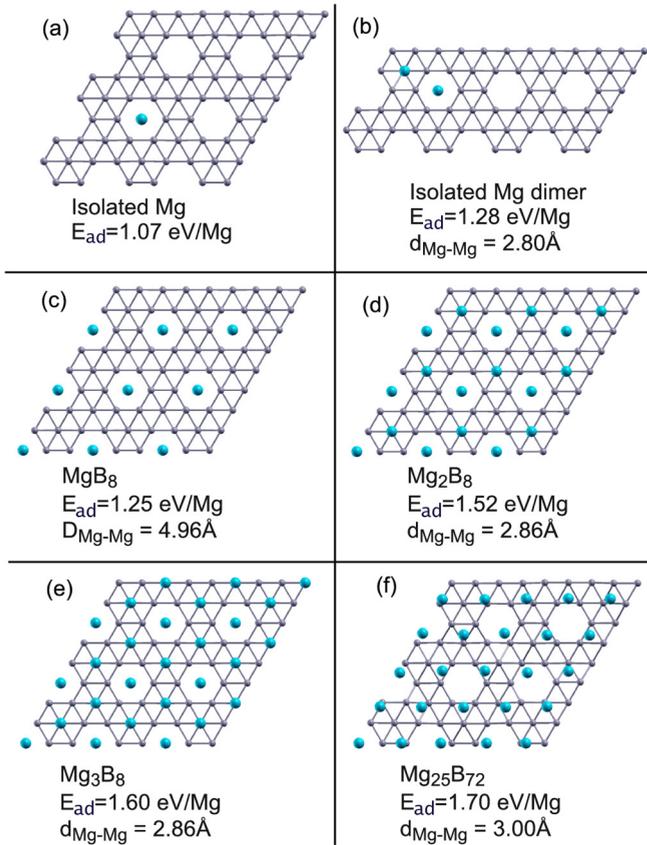
FIG. 3. Structures, adsorption energies, and Mg-Mg distances for six Mg-doped α-sheet structures: (a) isolated Mg, (b) Mg dimer, (c) MgB_8, (d) Mg_2B_8, (e) Mg_3B_8, and (f) $Mg_{25}B_{72}$. Large blue balls are Mg, small gray balls are B.

Mg-doped boron sheets. We define the adsorption energy per Mg for a particular 2D boron sheet as

$$E_{\text{ad}} = (E_B - E_{\text{doped}})/N_{\text{Mg}} + E_{\text{Mg}},$$

where E_{doped} is the total energy of the Mg-doped boron sheet, E_B is the energy of the boron sheet in the same simulation cell but with Mg removed, N_{Mg} is the number of adsorbed Mg atoms in the simulation cell, and E_{Mg} is the energy of an isolated Mg atom. Thus E_{ad} is positive, and larger E_{ad} corresponds to stronger binding of Mg to the boron subsystem.

We begin with Mg-doped α sheets. First, we check the convergence of E_{ad} versus the size of the periodic supercell. We find that E_{ad} for a single Mg is converged to within 5 meV/Mg for a 2×2 supercell (referenced to the 8-atom primitive cell of the α sheet). Next, we investigate the preferred adsorption site for the Mg. By starting relaxations from a large number of symmetry inequivalent Mg positions, we find that the position above the center of a hexagonal hole in the α boron sheet, shown in Fig. 3(a), is the most stable for an isolated Mg atom with $E_{\text{ad}} = 1.07$ eV/Mg. Other sites are at least 0.4 eV/Mg less stable.

Moving beyond isolated Mg, we study two Mg atoms on the α sheet in a 4×2 supercell. We search for the most stable structure for this pair by starting relaxations at many initial configurations including cases where the Mg are on opposite sides of the sheet. We find that the two Mg prefer to be on the

same side of the sheet, are attracted to each other, and form a dimer with a bond length of 2.80 Å [see Fig. 3(b)] and a dimer binding energy of 0.21 eV/Mg (compared to two isolated Mg on an α sheet). For comparison, the Mg-Mg dimer in vacuum has a computed LDA bond length of 3.40 Å [31].

Our final investigations on the α sheet involve a variety of 2D Mg meshes on top of the sheet at varying areal Mg densities. Figures 3(c)–3(f) show four example structures. The simplest 2D Mg structure is to place one Mg above the center of each hexagonal hole [Fig. 3(c)] with $E_{\text{ad}} = 1.25$ eV/Mg. When we increase the Mg fraction and put additional Mg on the triangular regions of the α sheet, we obtain hexagonal [Mg_2B_8 in Fig. 3(d)] and triangular [Mg_3B_8 in Fig. 3(e)] Mg lattices. These two configurations have E_{ad} of 1.52 eV/Mg and 1.60 eV/Mg which are about 0.5 eV/Mg more stable than an isolated Mg. In brief, Mg atoms on the α sheet attract each other and prefer to form dense 2D lattices on top of the α sheet instead of remaining isolated. After searching over many configurations, our current guess for the most optimal adsorption energy is $Mg_{25}B_{72}$ [Fig. 3(f)]: it has $E_{\text{ad}} = 1.70$ eV/Mg and is the most stable structure we have found to date. The Mg-Mg bond length in $Mg_{25}B_{72}$ is about 3.00 Å which is very close to the Mg-Mg bond length of 2.99 Å we calculate for a freestanding 2D triangular lattice of Mg atoms. Hence, we can say that the absorbed Mg on the boron sheet in this optimal case are forming covalent bonds.

As noted above, Mg on hexagonal boron sheets behaves quite differently. We find that the most stable isolated adsorption site is above the center of each hexagon with a strong binding energy of $E_{\text{ad}} = 3.56$ eV/Mg for an isolated Mg. In addition, we find that the Mg-Mg interaction on the hexagonal boron sheet is repulsive so that isolated Mg has the largest E_{ad}.

With these two cases described in some detail, we now summarize our results for a number of other boron sheets. We find that for sheets with $\eta < 1/7$, the absorbed Mg attract each other, and that the structures with the highest Mg adsorption energies have densely packed Mg lattices with Mg-Mg bond lengths close to that of the optimum for an isolated 2D Mg sheet (2.99 Å). On the other hand, for $\eta > 1/7$, the Mg-Mg interaction is repulsive and isolated Mg atoms are energetically preferred.

Charge transfer. It turns out that these interesting Mg-Mg interactions are best explained by a charge transfer picture. In MgB_x systems, we expect Mg to donate electrons to the more electronegative boron subsystem and become positively charged. The amount of electron transfer is driven by the Fermi level difference between the Mg and boron subsystems. For an isolated Mg atom, we take the Fermi level to be the energy of the $3s^2$ atomic level so that the difference in Fermi level is actually determined by the Fermi level of the boron sheet. Figure 4 shows the behavior of the Fermi level versus η for a variety of boron sheets: the Fermi level drops monotonically with increasing η. Hence, we expect that Mg donates fewer electrons to small-η boron sheets and more electrons to large-η boron sheets.

We verify this expectation with explicit calculations. Figure 5 shows the calculated electron transfer from Mg to a variety of boron sheets based on two distinct electron-counting schemes: the occupations of Löwdin orbitals [32] and the occupations of Maximally Localized Wannier Functions
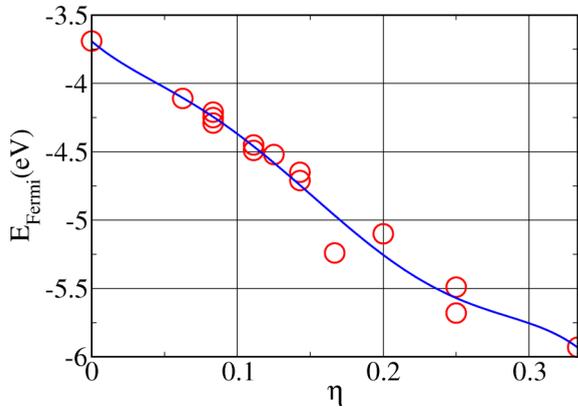
FIG. 4. Fermi level of boron sheets with respect to vacuum from DFT-LDA calculations versus hexagonal hole density η. The red circles are the calculated data, and the blue solid curve is a fit to guide the eye.

TABLE I. Curvature energies for nanotubes made from the Mg-doped α sheet with stoichiometry MgB_8. E_{Mg} is the curvature energy for the Mg subsystem in eV per Mg. E_B is the curvature energy for the B subsystem in eV per B_8. E_{sum} is the sum of E_{Mg} and E_B. E_{curv} is the actual curvature energy for these Mg boride nanotubes in eV/MgB_8.

	E_{Mg}	E_B	E_{sum}	E_{curv}
(6,0)	-0.38	0.37	-0.01	0.00
(8,0)	-0.35	0.22	-0.13	-0.15
(10,0)	-0.25	0.15	-0.10	-0.10
(3,3)	-0.76	0.45	-0.31	-0.30
(4,4)	-0.48	0.26	-0.22	-0.15
(5,5)	-0.30	0.17	-0.13	-0.08
(6,6)	-0.22	0.12	-0.10	-0.04
(8,8)	-0.14	0.07	-0.07	-0.02

[21,28–30]. Obviously the two methods differ quantitatively, but both show a monotonic increase of electron transfer with η. Therefore, on small-η boron sheets, the Mg atoms donate few electrons and remain close to neutral: this explains their preference for aggregation and formation of covalent bonds in a manner similar to neutral and isolated Mg atoms. However, when placed on large-η boron sheets, the Mg become quite ionized and positively charged so that Coulomb repulsion dominates Mg-Mg interactions and the Mg prefer to be isolated.

Mg on model boron nanotubes. Having understood Mg on 2D boron sheets, we now can explain the behavior of the model Mg-doped boron nanotubes. When we construct a MgB_x nanotube by curving the parent 2D sheet, the curvature changes the Mg-Mg distances compared to the flat sheet. If the Mg are outside the nanotube, their separations are increased compared to the parent 2D sheet; if they are inside the nanotube, their separations are decreased. For small η, the Mg-Mg interaction is attractive so that the Mg atoms prefer to aggregate: placing the Mg inside the nanotube is favorable. If

FIG. 5. Electron transfer in e/Mg from absorbed Mg to boron sheets calculated using maximally localized Wannier functions (blue circles) and Löwdin orbitals (red squares) for a variety of boron sheets as a function of the hexagonal hole density η of the sheets.

the Mg-Mg attraction is strong enough to overcome the energy cost to curve the boron subsystem, we find negative curvature energy as per Fig. 1. Oppositely, nanotubes stemming from large-η boron sheets have repulsive Mg-Mg interactions: when placed outside the nanotube, the increased Mg-Mg separation due to curvature is energetically favorable. Again, it can overwhelm the cost of curving the boron subsystem and lead to negative curvature energy as per Fig. 2.

To support this rationalization, we consider MgB_8 nanotubes (Mg doped on curved α sheets) with the Mg inside so that we have negative curvature energies. To verify that Mg-Mg interactions lead to negative curvature energies, we approximate the curvature energy of the MgB_8 nanotube as the sum of the curvature energy of the boron nanotube subsystem and the Mg subsystem treated separately (i.e., we assume that the bonding and electron transfer between Mg and boron does not change with curvature). For this analysis, no relaxations are performed: we take the final structure of the nanotube and remove atoms to create the separate Mg or boron subsystems and compute their total energies. Table I shows the resulting energies and compares them to the actual curvature energies. This simple model is impressively accurate and, more importantly, confirms that the Mg-Mg interactions are the dominant force behind the existence of negative curvature energy in these nanotubes.

More complex structures. The above results show that charge transfer from Mg to boron in MgB_x sheets and nanotubes has a profound effect on the nature of the Mg-Mg interactions: the nature of the 2D boron subsystem can tune the interaction to be either repulsive or attractive. For the model nanotubes above, the Mg-Mg interactions were strong enough to lead to negative curvature energy. However, given the idealized nature of the systems, the existence or relevance of negative curvature energy in more complex and more realistic MgB_x nanotubular structures is not obvious.

The model calculations can be made more realistic in a few distinct ways. First, in the above calculations, all the Mg on the 2D sheets were adsorbed on one side of the sheet so that, in the resulting nanotubes, all the Mg were either inside or outside the nanotube. Are such reference 2D sheets realistic or appropriate? Namely, if a lower-energy 2D MgB_x sheet exists where Mg are adsorbed on both sides of the boron subsystem, will this added stability of the 2D sheet invalidate the existence

negative curvature energy? If we restrict ourselves to 2D sheets where the Mg are evenly space in the xy plane but can adsorb above or below the boron subsystem, the situation turns out to remain unchanged and negative curvature energy should continue to exist. Specifically, we have examined 2×2 supercells of the MgB_8 sheet (Fig. 1) and MgB_2 sheet (Fig. 2) and computed total energies for all distinct permutations of the Mg being above and below the boron subsystem. For the α-based MgB_8 sheet, the Mg prefer to be all on the same side of the 2D sheet which is expected based on the attractive Mg-Mg interactions. For the hexagonal MgB_2 case where Mg-Mg interactions are repulsive, putting some Mg above and the rest below the boron subsystem is energetically favorable as expected. However, the magnitude of the energy lowering turns out to be small at -0.02 eV/atom. On the energy scales of Fig. 2, changing the reference energy of the parent sheet (i.e., the zero of energy) by this amount does not change our conclusion about the existence of negative curvature energy for this class of nanotubes. Hence, under the assumption of uniformly distributed Mg on the boron subsystem, we expect MgB_x nanotubes to display negative curvature energy.

For nanotubes based on large-η boron sheets where Mg-Mg interactions are repulsive, the Mg want to stay far apart: we expect homogeneous Mg distributions and hence negative curvature energy to exist. However, for the systems where the Mg-Mg interactions are attractive (e.g., the α-based MgB_8 systems of Fig. 3), we expect that the Mg would prefer to aggregate into regions of higher areal density to lower the total energy. For 2D sheets, this is clear from the computed adsorption energies above. For nanotubes, this is a sensible speculation that requires verification in future works. For low-η sheets and nanotubes, we expect to find phase separation into Mg-rich and Mg-poor regions at thermodynamic equilibrium.

Whether negative curvature energy exists from a thermodynamic viewpoint in such inhomogeneous systems is an open question for future work. However, we point out that thermodynamic considerations may not be the only relevant factors: the kinetics of the growth process (e.g., growing a MgB_x nanotube inside a confining porous scaffold) may hinder Mg diffusion to an extent where the phase separation is incomplete or nonexistent. In our mind, further theoretical and experimental work is needed to understand the structure of MgB_x nanotubes built from boron sheets with small η which have attractive Mg-Mg interactions.

Conclusions. We have examined a number of MgB_x 2D sheets and nanotubes and elucidated the interplay of electron transfer, Mg-Mg interactions, and the existence of negative curvature energy in resulting nanotubes. The degree of electron transfer from Mg to the boron subsystem depends strongly on the hole density η of the 2D boron sheet. The degree of electron transfer controls the nature of Mg-Mg interactions: covalent attraction for small electron transfer and ionic repulsion for large electron transfer. These Mg-Mg interactions can be strong enough to overwhelm the energy cost of curving the underlying boron 2D sheet and can lead to negative curvature energy for cases where the Mg are adsorbed homogeneously on the surface of the boron subsystem. The possibility of heterogenous Mg distributions and phase separation into Mg-poor and Mg-rich regions underlines the need for future work on more complex MgB_x systems as well as improved understanding of the kinetics of the nanotube growth process. Should negative curvature exist in these more complex structures, it would provide an unusual method to stabilize nanotubular materials with extremely high curvatures and small diameters.

[1] R. Saito, G. Dresselhaus, and M. S. Dresselhaus, *Physical Properties of Carbon Nanotubes* (Imperial College Press, London, 1998).

[2] N. Chopra, R. J. Luyken, D. Cherrey, V. H. Crespi, M. L. Cohen, S. G. Louie, and A. Zettl, Science **269**, 966 (1995).

[3] A. Rubio, J. L. Corkill, and M. L. Cohen, Phys. Rev. B **49**, 5081 (1994).

[4] D. Ciuparu, R. F. Klie, Y. Zhu, and L. Pfefferle, J. Phys. Chem. B **108**, 3967 (2004).

[5] H. Tang and S. Ismail-Beigi, Phys. Rev. Lett. **99**, 115501 (2007).

[6] X. Yang, Y. Ding, and J. Ni, Phys. Rev. B **77**, 041402(R) (2008).

[7] H. Tang and S. Ismail-Beigi, Phys. Rev. B **82**, 115412 (2010).

[8] N. Hamada, S. I. Sawada, and A. Oshiyama, Phys. Rev. Lett. **68**, 1579 (1992).

[9] X. Blase, L. X. Benedict, E. L. Shirley, and S. G. Louie, Phys. Rev. Lett. **72**, 1878 (1994).

[10] A. K. Singh, A. Sadrzadeh, and B. I. Yakobson, Nano Lett. **8**, 1314 (2008).

[11] D. H. Robertson, D. W. Brenner, and J. W. Mintmire, Phys. Rev. B **45**, 12592 (1992).

[12] I. Boustani and A. Quandt, Europhys. Lett. **39**, 527 (1997).

[13] A. Gindulyte, W. N. Lipscomb, and L. Massa, Inorg. Chem. **37**, 6544 (1998).

[14] L. A. Chernozatonskii, JETP Lett. **74**, 335 (2001).

[15] V. Pokropivny, Int. J. Nanotechnol. **1**, 170 (2004).

[16] V. V. Ivanovskaya, A. N. Enjashin, A. A. Sofronov, Y. N. Makurin, N. I. Medvedeva, and A. L. Ivanovskii, J. Mol. Struct., Theochem **625**, 9 (2003).

[17] D. L. V. K. Prasad and E. D. Jemmis, J. Mol. Struct.: THEOCHEM **771**, 111 (2006).

[18] S. Saito, S. G. Louie, and M. L. Cohen, J. Phys. Soc. Jpn. **76**, 043707 (2007).

[19] P. B. Sorokin, L. A. Chernozatonskii, P. V. Avramov, and B. I. Yakobson, J. Phys. Chem. C **114**, 4852 (2010).

[20] E. Iyyamperumal, F. Fang, A.-B. Posadas, C. Ahn, R. F. Klie, Y. Zhao, G. L. Haller, and L. D. Pfefferle, J. Phys. Chem. C **113**, 17661 (2009).

[21] H. Tang and S. Ismail-Beigi, Phys. Rev. B **80**, 134113 (2009).

[22] P. Hohenberg and W. Kohn, Phys. Rev. **136**, B864 (1964).

[23] W. Kohn and L. J. Sham, Phys. Rev. **140**, A1133 (1965).

[24] M. C. Payne, M. P. Teter, D. C. Allan, T. A. Arias, and J. D. Joannopoulos, Rev. Mod. Phys. **64**, 1045 (1992).

[25] P. Giannozzi, S. Baroni, N. Bonini, M. Calandra, R. Car, C. Cavazzoni, D. Ceresoli, G. L. Chiarotti, M. Cococcioni, I. Dabo, A. D. Corso, S. d. Gironcoli, S. Fabris, G. Fratesi, R. Gebauer, U. Gerstmann, C. Gougoussis, A. Kokalj, M. Lazzeri, L. Martin-Samos, N. Marzari, F. Mauri, R. Mazzarello, S. Paolini, A. Pasquarello, L. Paulatto, C. Sbraccia, S. Scandolo, G. Sclauzero, A. P. Seitsonen, A. Smogunov, P. Umari, and R. M. Wentzcovitch, J. Phys.: Condens. Matter **21**, 395502 (2009).

[26] J. P. Perdew and A. Zunger, Phys. Rev. B **23**, 5048 (1981).

[27] N. Troullier and J. L. Martins, Phys. Rev. B **43**, 1993 (1991).

[28] N. Marzari and D. Vanderbilt, Phys. Rev. B **56**, 12847 (1997).

[29] I. Souza, N. Marzari, and D. Vanderbilt, Phys. Rev. B **65**, 035109 (2001).

[30] A. A. Mostofi, J. R. Yates, Y.-S. Lee, I. Souza, D. Vanderbilt, and N. Marzari, Comput. Phys. Commun. **178**, 685 (2007).

[31] I. C. Gerber and J. G. Angyan, Chem. Phys. Lett. **416**, 370 (2005).

[32] P.-O. Löwdin, J. Chem. Phys. **18**, 365 (1950).